

Energy, Direction and Vertex Reconstruction for a Proposed Water Cherenkov Neutrino Detector at Oak Ridge National Laboratory

Ching Yu Leung^{1, a}

¹The Chinese University of Hong Kong

University of Tokyo Research Internship Program 2024, Yokoyama-Nakajima Research Group

(Dated: 3rd September 2024)

In order to extract information from the neutrino burst of the next detectable core-collapse supernova, cross sections of different neutrino interactions need to be measured. While extensive research has been conducted on inverse beta decay the primary neutrino interaction of water Cherenkov detectors, there is no existing measurements of cross sections on $\nu_e - {}^{16}\text{O}$ charged current (CC) and $\nu_x - {}^{16}\text{O}$ neutral current (NC) interactions in low energy range, which are something a proposed water Cherenkov detector at Oak Ridge National Laboratory hopes to measure. The detector features a cylindrical water tank with a radius of 20 cm and a height of 80 cm, with 7 PMTs installed on the top and the bottom respectively. This report introduces possible methods for energy, direction and vertex reconstructions, and looks for improvements on the configurations for better reconstruction. To evaluate the performance of the reconstruction methods, simulations were conducted using Geant4 by shooting electrons inside the water tank. Overall, electron energy and polar angle of its moving direction can be determined by the total number of PMT hits and the ratio of hits between the top and bottom PMTs respectively. Z coordinate of an electron can be deduced from the first PMT hit time on either the top or the bottom, depending on the reconstructed polar angle. By introducing a highly reflective optical surface inside the water tank, the performance of energy reconstruction is enhanced significantly. Besides, PMT separation at 14 cm is also found to yield more signals.

I. INTRODUCTION

The motivation of this research and an introduction of the proposed detector is given here.

A. Supernova Neutrino Physics

Information from core-collapse supernova can contribute to wide variety of physics topics, including core collapse mechanism, nucleosynthesis and quark phase transitions [1–3]. Since the last detectable core-collapse supernova, the renowned SN1987A, it has been already approximately four decades. In contemporary neutrino detectors, thousands of events are expected to be detected from the neutrino burst of a galactic core-collapse supernova (GCCS). While physicists are fervently waiting for the next GCCS, which are expected to occur 1.63 ± 0.46 times per century [4], more study on the neutrino cross sections are necessary in order to interpret the supernova neutrino burst signals.

In water Cherenkov detector like Super-Kamiokande, the predominant signal stems from inverse beta decay. Nevertheless, there are also signals from $\nu_e - {}^{16}\text{O}$ CC and $\nu_x - {}^{16}\text{O}$ NC interactions, which provide sensitivity information to the ν_e and ν_x neutrino fluxes and which we want to distinguish from inverse beta decay. Nevertheless, there is no existing measurement on the cross sections of these two interactions in the few-tens-of-MeV energy range [5]. Consequently, a proposal has been put forth for the construction of a water Cherenkov

neutrino detector at Oak Ridge National Laboratory, specifically intended for the measurement of these cross sections.

B. Detector Structure and Setup

Figure 1 is the simulated detector in Geant4, which consists of a cylindrical water tank made of acrylite with a radius of 20 cm and a height of 80 cm. Above and below the water tank are 7 PMTs with a radius of 3.81 cm respectively. The optimal PMT separation is subject to test. Surrounding the tank is a sodium iodide layer of thickness 5 cm, which is further enveloped by a 10.16 cm thick lead shield and a 5.08 cm thick Veto.

In contrast to Super-Kamiokande, where the inner surface of the water tank is coated with a highly absorptive optical surface to ensure detected photons originates directly from a charged particle, it is unnecessary in this small water Cherenkov detector because there is no hope to reconstruct the vertex and direction of the charged particle through the directionality of photons given limited number of PMTs. Conversely, introducing a reflective optical surface on the inner curved surface could potentially benefit energy reconstruction by increasing the total number of yields. However, it requires further testing.

The proposed detector will be installed at around 20 m away from Spallation Neutron Source (SNS) at Oak Ridge. SNS serves as a neutrino source for cross sections measurement. When a high energy proton beam is directed towards the mercury target, stationary positive pion is created and subsequently decays through the following process [6].

^a 1155176801@link.cuhk.edu.hk

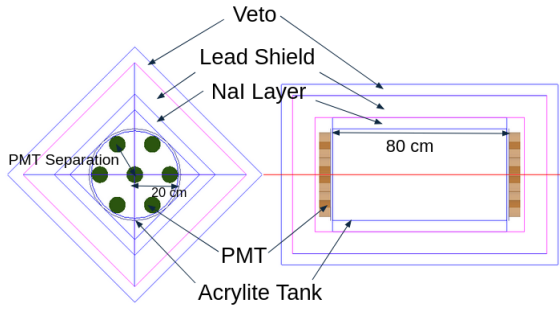


Figure 1. Top view and side view of the simulated detector in Geant4

$$\pi^+ \rightarrow \nu_\mu + \mu \quad (1)$$

$$\mu^+ \rightarrow \bar{\nu}_\mu + \nu_e + e^+ \quad (2)$$

As a result, ν_μ , $\bar{\nu}_\mu$ and ν_e are created from the source.

II. PHYSICS BACKGROUND

A. Cherenkov Radiation

Akin to sonic boom which occurs when an object moves faster than the speed of sound within a given medium, Cherenkov radiation is emitted when an electrically charged particle moves faster than the speed of light within that medium. For example, in water with a refractive index of 1.33, a charged particle must travel at speed exceeding 0.75 times the speed of light to induce Cherenkov radiation. The angle of emission denoted as theta in figure 2 is determined by the following formula.

$$\cos \theta = \frac{c}{nv} \quad (3)$$

For a highly relativistic particle, the angle is around 40° . As the particle loses energy through scattering and emission of Cherenkov radiation, the angle is reduced gradually.

B. Detection of $\nu_e - {}^{16}\text{O}$ CC and $\nu_x - {}^{16}\text{O}$ NC Interaction

Various interaction modes exist for $\nu_e - {}^{16}\text{O}$ CC and $\nu_x - {}^{16}\text{O}$ NC as shown in table I and table II. The resultant nuclei are usually excited, leading to subsequent de-excitation via emission of gamma radiation. The gamma radiation may then undergo Compton scattering, thereby prompting a relativistic electron that induces Cherenkov radiation. For $\nu_e - {}^{16}\text{O}$ CC, the excited nucleus is usually accompanied by a relativistic electron, which is responsible for the production of Cherenkov radiation as well.

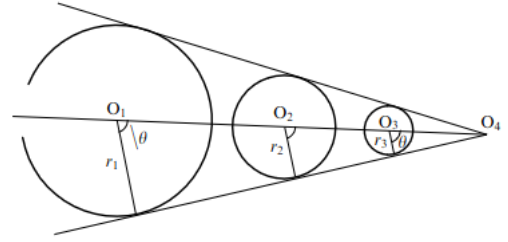


Figure 2. An illustration of how Cherenkov radiation is emitted adopted from [7]. O_1 , O_2 , O_3 and O_4 are snapshots of a charged particle at different moment as it moves to the right. At each moment, Cherenkov radiation is emitted at an angle θ , resulting in the conical surface of Cherenkov radiation.

Neutrino reaction	$\sigma, T=4$ MeV	$\sigma, T=8$ MeV
total	1.91 (-1)	1.37 (+1)
${}^{16}\text{O}(\nu_e, e^- p){}^{15}\text{O}(\text{g.s.})$	1.21 (-1)	6.37 (+0)
${}^{16}\text{O}(\nu_e, e^- p \gamma){}^{15}\text{O}^*$	4.07 (-2)	3.19 (+0)
${}^{16}\text{O}(\nu_e, e^- n p){}^{14}\text{O}^*$	3.92 (-4)	1.76 (-1)
${}^{16}\text{O}(\nu_e, e^- p p){}^{14}\text{N}^*$	2.61 (-2)	3.26 (+0)
${}^{16}\text{O}(\nu_e, e^- \alpha){}^{12}\text{N}^*$	1.16 (-3)	1.31 (-1)
${}^{16}\text{O}(\nu_e, e^- p \alpha){}^{11}\text{C}^*$	2.17 (-3)	5.66 (-1)
${}^{16}\text{O}(\nu_e, e^- n \alpha){}^{11}\text{N}(p){}^{10}\text{C}^*$	1.11 (-6)	3.28 (-3)

Table I. Table of CC neutrino induced reactions on ${}^{16}\text{O}$ and their partial cross section with temperatures 4 MeV and 8 MeV and zero chemical potential [8]. Cross sections are given in unit of 10^{-42}cm^2 . Inside the parentheses are the exponents.

Neutrino reaction	$\sigma, T=8$ MeV
total	5.19 (+0)
${}^{16}\text{O}(\nu, \nu' \gamma){}^{16}\text{O}^*$	3.19 (-3)
${}^{16}\text{O}(\nu, \nu' n){}^{15}\text{O}(\text{g.s.})$	9.73 (-1)
${}^{16}\text{O}(\nu, \nu' p){}^{15}\text{N}(\text{g.s.})$	1.85 (+0)
${}^{16}\text{O}(\nu, \nu' n \gamma){}^{15}\text{O}^*$	3.48 (-1)
${}^{16}\text{O}(\nu, \nu' n n){}^{14}\text{O}^*$	6.11 (-3)
${}^{16}\text{O}(\nu, \nu' n p){}^{14}\text{N}^*$	4.40 (-1)
${}^{16}\text{O}(\nu, \nu' p \gamma){}^{15}\text{N}^*$	1.29 (+0)
${}^{16}\text{O}(\nu, \nu' p p){}^{14}\text{C}^*$	8.35 (-2)
${}^{16}\text{O}(\nu, \nu' p \alpha){}^{11}\text{B}^*$	9.15 (-2)
${}^{16}\text{O}(\nu, \nu' n \alpha){}^{11}\text{C}^*$	3.88 (-2)

Table II. Table of NC neutrino induced reactions on ${}^{16}\text{O}$ and their partial cross section with a temperature 8 MeV and zero chemical potential [8]. Cross sections are given in unit of 10^{-42}cm^2 . Inside the parentheses are the exponents.

III. SIMULATION RESULT

Since electrons are always the resulting product in the above neutrino interactions and are where the Cherenkov radiation comes from, simulations were done by generating electrons inside the water tank. Each data point is the average of 100000 trials.

A. Energy Reconstruction

Simulations were done by shooting electrons of specific energy ranging from 1 MeV to 40 MeV. PMTs are separated by 16 cm. Detectors with optical surfaces of 30%, 50%, 80% and 98% reflectivity are compared with the detector with no optical surface. Note that reflectivity is defined to be the probability of photons being reflected while the probability of photons being absorbed is 1-reflectivity. No photons can pass through an optical surface.

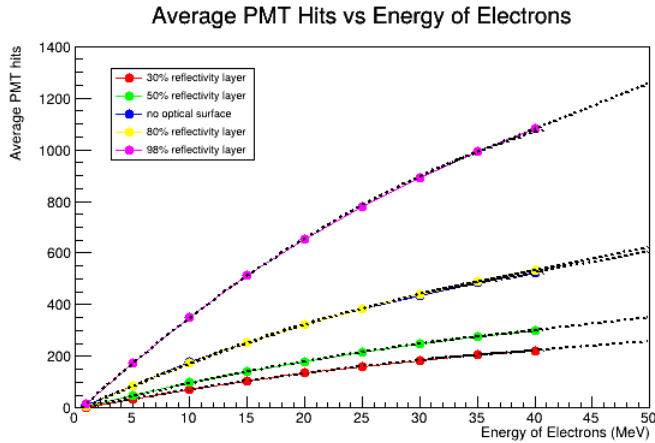


Figure 3. Average PMT hits as a function of electron energy.

A simple energy reconstruction based on the average number of PMT hits can be done by using a hybrid function of a quadratic function (for electron energy smaller or equal to 40 MeV) and a linear function (for electron energy greater than 40 MeV) as shown in figure 3. Notably, the detector with a 98% reflectivity optical surface yields the most signals, and the detector with no optical surface has similar average PMT hits as the one with a 80% reflectivity optical surface.

The bias of reconstructed energy against true electron energy is plotted in figure 4. It is noticeable that biases, defined as the average of the reconstructed energy minus true electrons energy, decrease with reflectivity and the detector with a 98% reflectivity optical surface has the least bias. The origin of biases is not well understood though. A naive guess is that it is due to the non-linear relation between average PMT hits and energy of electrons. It is left as a future work.

Figure 5 shows the resolution of reconstructed energy as a

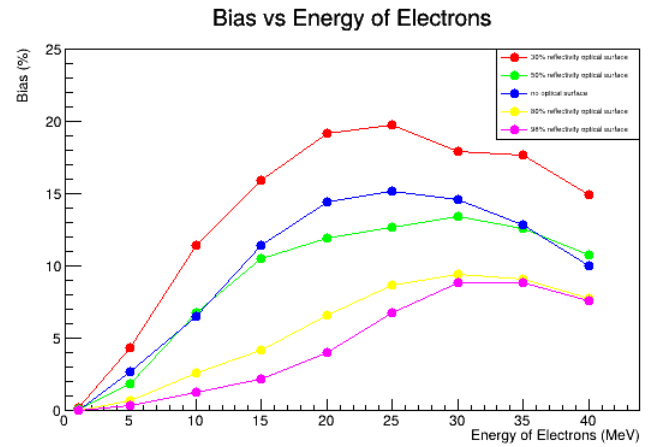


Figure 4. Bias as a function of electron energy

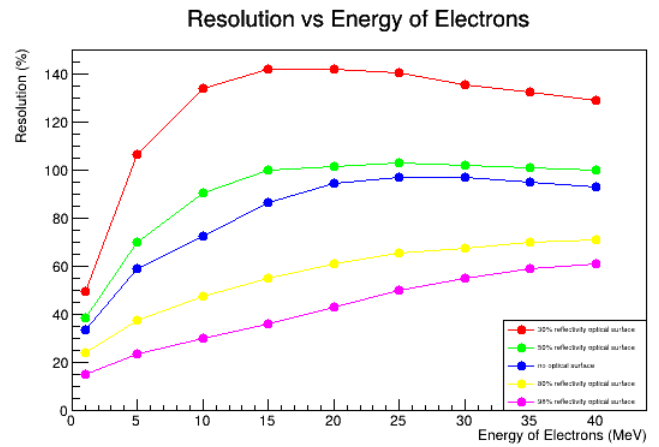


Figure 5. Resolution as a function of electron energy

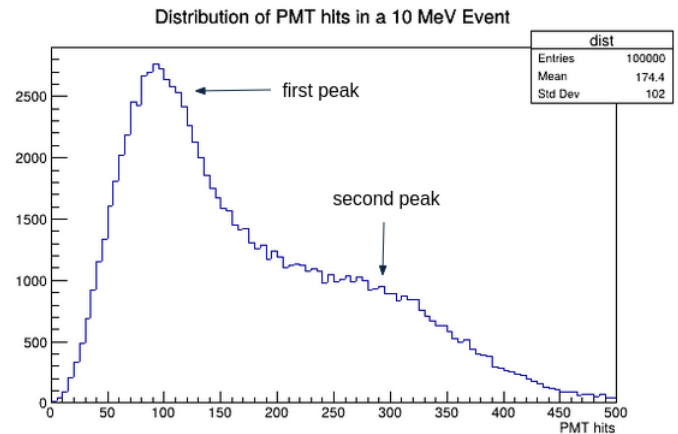


Figure 6. Distribution of PMT hits of the detector with no optical surface when 10 MeV electrons were simulated.

function of true electron energy. Again, resolution, defined as the standard deviation of the distribution of reconstructed energy minus true electrons energy, appears to decrease with reflectivity and the detector with a 98% reflectivity optical

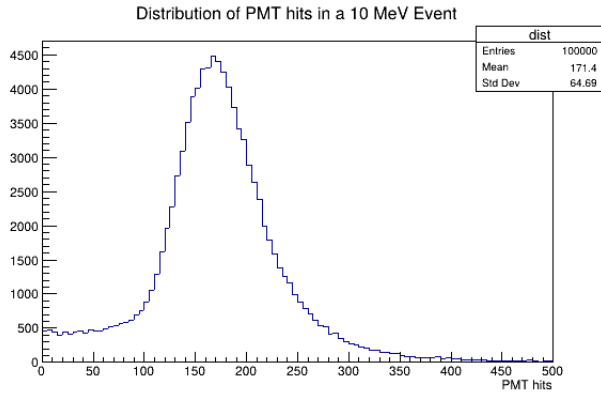


Figure 7. Distribution of PMT hits of the detector with 80% reflectivity optical surface when 10 MeV electrons were simulated.

surface has the least resolution. It is evident that the detector with no optical surface has a larger resolution than the detector with a 80% reflectivity optical surface although they have almost the same average PMT hits. The reason is attributed to the shape of their distributions of PMT hits, which are plotted in figure 6 and 7. The distribution of the detector with no optical surface has double peaks while the distribution with an optical surface is Gaussian-like, which explains why the former has a larger resolution. The two peaks belong to two possibilities in each simulation. Usually, most of the Cherenkov radiation emitted passes through the acrylic water tank, subsequently absorbed by the lead shield. However, in some cases, when Cherenkov radiation are directed relatively parallel to the acrylic surface, lots of the photons undergo total internal reflection and are trapped inside the water tank, which in turn yield more signals. One feature of this case is that those photons in general undergoes multiple times of total internal reflection before being detected and absorbed by PMTs. Adding an optical surface reduces the PMT hits of the second case by absorbing photons going through multiple reflection and also raises the PMT hits in the first case by reflecting photons that otherwise passes through the acrylic tank. As a result, two peaks approach each other and resemble a single peak in figure 7.

The biggest takeaway in this session is that adding a 98% reflectivity optical surface helps reduce the bias and resolution significantly, allowing a better energy reconstruction.

To further increase the number of signals, we need to find the optimal PMT separation. The detector with a 98% reflectivity optical surface was used in the simulation. When 20 MeV electrons were simulated, PMTs separated by 14 cm are found to yield the most signals as shown in figure 8, similarly for other electron energy.

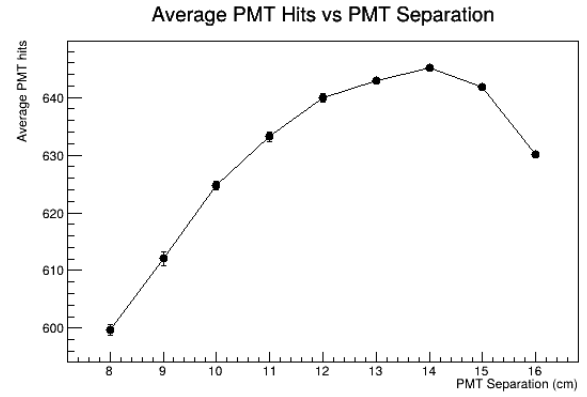


Figure 8. Average PMT hits as a function of PMT separation. 20 MeV electrons were simulated.

B. Direction Reconstruction

Simulations were conducted by shooting 5 MeV electrons emitted at a specific polar angle (denoted by the black curve in figure 9) or at a specific z coordinate (denoted by the red curve in figure 9) within the water tank coated with a 98% reflectivity optical surface. PMTs are separated by 16 cm. Note that polar angle is defined to be the angle with respect to the z axis.

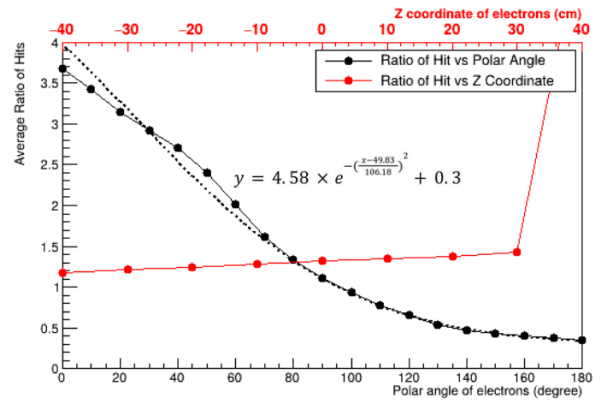


Figure 9. Average ratio of PMT hits on the top to the bottom as a function of polar angle and z coordinate of electrons

Figure 9 shows the relation between the average ratio of PMT hits on the top to the bottom and the polar angle as well as the relation between the average ratio and the z coordinate of electrons. The fitted curve in figure 9 allows polar angle reconstruction based on the ratio of hits. The dependency on z coordinate can be neglected unless the electron is generated close to $z = 40$ cm, where the ratio increases significantly. The notable rise is suspicious because such behaviour is not observed at $z = -40$ cm and may suggest that there is asymmetry between the upper and the lower part of the detector. To ensure there is no asymmetry, the ratio was redefined as PMT hits on the bottom to the top in figure 10. The plot is a reflection of figure 9, indicating no asymmetry.

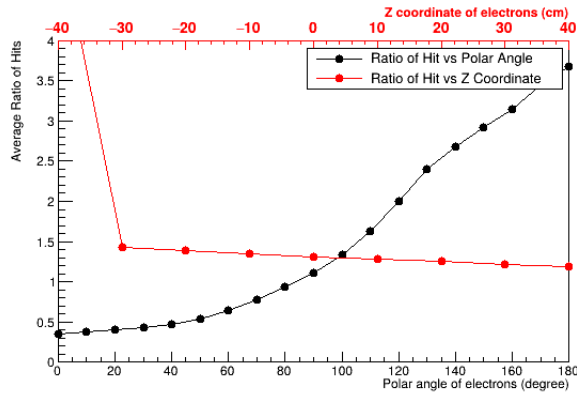


Figure 10. Average ratio of PMT hits on the bottom to the top as a function of polar angle and z coordinate of electrons

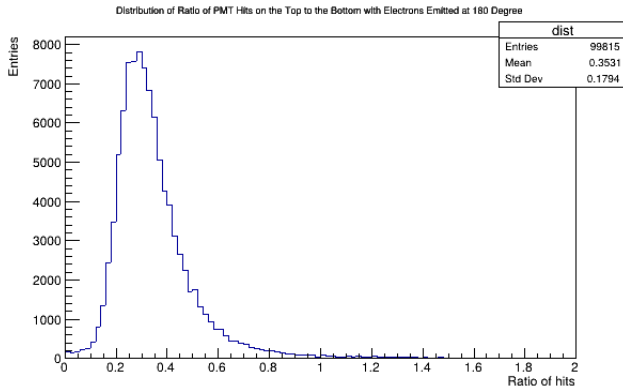


Figure 11. Distribution of ratio of hits with electrons emitted at a 180° polar angle

Due to limited time, I did not perform detailed bias and resolution analyses like the one I did for energy reconstruction. Instead, I focused on the distribution of PMT hits, of which the standard deviation is closely related to the resolution. Although we do not have a qualitative goal for the standard deviation, a Gaussian-like distribution as depicted in figure 11 is what we aim for.

The main takeaway in this section is that the z-dependence of ratio of hits is relatively small in most the case, and we can reconstruct the polar angle using the ratio of hits.

C. Vertex Reconstruction

Simulations were done by shooting 5 MeV electrons at a specific z coordinate and at a polar angle uniformly distributed from 0° to 90° (denoted by the black curve in figure 12) or from 90° to 180° (denoted by the black curve in figure 13) as well as at a specific polar angle (denoted by the red curves in figure 12 and 13). The inner curved surface of the water tank is coated with a 98% reflectivity optical

surface and the PMTs are again separated by 16 cm.

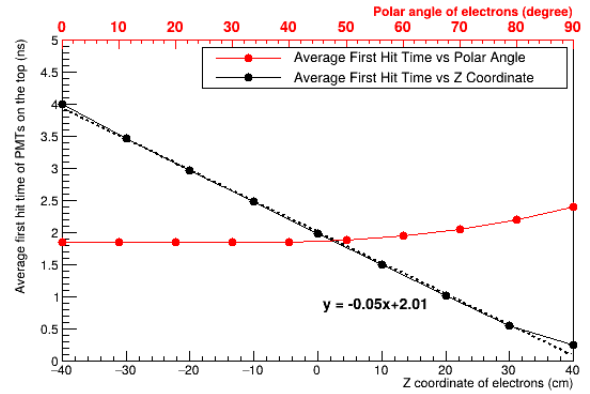


Figure 12. Average first hit time of PMTs on the top as a function of z coordinate and polar angle of electrons

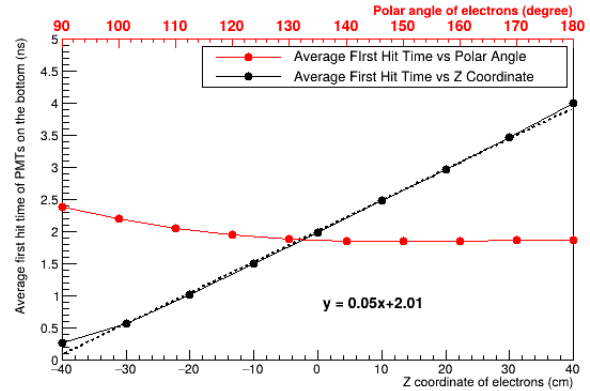


Figure 13. Average first hit time of PMTs on the bottom as a function of z coordinate and polar angle of electrons

In figure 12, the main focus is the relation between the average first hit time of PMTs on the top and the z coordinate of electrons emitted at a polar angle uniformly distributed from 0° to 90° while figure 13 demonstrates the relation between the average first hit time of PMTs on the bottom and the z coordinate of electrons emitted at a polar angle uniformly distributed from 90° to 180° . In practice, if the reconstructed polar angle is greater than 90° , the straight line equation in figure 13 is used to reconstruct the z coordinate; otherwise the one in figure 12 is employed. The dependency of the average first hit time on the polar angle can be ignored for now. The reason of employing distinct first hit times, depending on the polar angle, is explained below.

As illustrated in figure 14, emission of an electron at around 40° induces Cherenkov radiation that moves straight towards the top or parallel to the curved surface, which gives the shortest hit time. Even if electrons are not initially emitted at this angle, after multiple scattering, their moving direction may still align with this angle. Consequently, in most of the

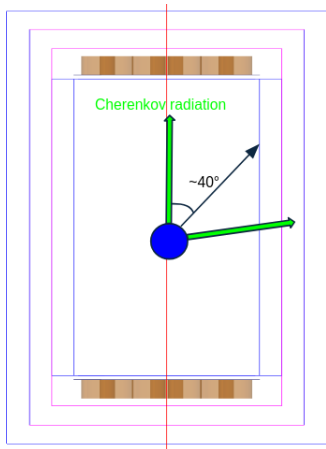


Figure 14. An illustration of emission of Cherenkov radiation that moves straight towards the top. Such radiation comes from a relativistic electrons that moves at a $\sim 40^\circ$ polar angle.

case, there is Cherenkov radiation directed straight towards the top, unless the electron is emitted at a much larger polar angle where such alignment is less probable. In such cases, the first hit time on the top may be slightly prolonged because no cherenkov radiation is emitted straight towards the top. Using the first hit time of the bottom PMTs is then more reliable. To conclude, for electrons emitted at a polar angle smaller than 90° , the first hit time of the top PMTs is a good parameter and for electron emitted at a polar angle larger than 90° , the first hit time of the bottom PMTs is more suitable. We will soon see that even the electron is emitted at around 90° , the first hit time on the top or the bottom is still prolonged, indicating that even after multiple scattering, the electron still fails to move at around 40° or 120° .

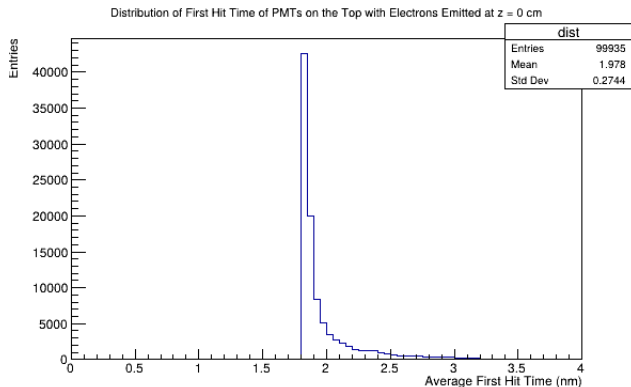


Figure 15. Distribution of first hit time of PMTs on the top when electrons is emitted at $z = 0$ cm and at a uniformly distributed polar angle from 0° to 90° .

Similar to direction reconstruction, the distribution of the first hit time is plotted in figure 15. A spike-like distribution indicates precise determination of the z coordinate is possible. Nevertheless, the short tail, stemming from electrons emitted

at a polar angle near 90° and fail to move in 40° even after scattering, may degrade the performance. In fact, we can see a slight dependency of the first hit time on the polar angle when it approximates 90° in figure 12 and 13 due to this reason. To mitigate this issue, a plot excluding electrons emitted at a polar angle greater than 50° is presented in figure 16. By doing so, the tail is removed.

To conclude, this method fails when the electron is emitted at a polar angle near 90° . In such cases, we may need separated method to reconstruct the z coordinate.

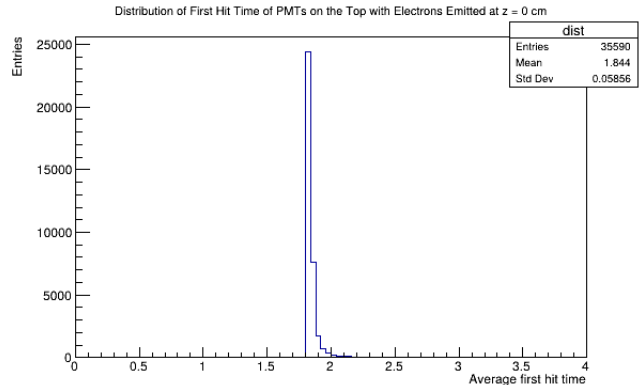


Figure 16. Distribution of first hit time of PMTs on the top when electrons is emitted at $z = 0$ cm and at a uniformly distributed polar angle from 0° to 50° .

IV. CONCLUSION

In summary, to measure the cross sections of $\nu_e - {}^{16}\text{O}$ CC and $\nu_x - {}^{16}\text{O}$ NC interactions in few-tens-of-MeV energy range, a water Cherenkov neutrino detector located at around 20 m away from the Spallation Neutron Source at Oak Ridge National Laboratory is proposed. Energy and direction can be reconstructed by the total number of PMT hits and ratio of PMT hits on the top to the bottom respectively. Vertex reconstruction using first hit time is possible under specific condition. By coating a 98% reflectivity optical surface on the inner curved surface of the water tank, performance of energy reconstruction is enhanced. PMTs are also found to work the best when separated by 14 cm.

V. ACKNOWLEDGEMENT

I would like to thank the University of Tokyo for organising UTRIP 2024, which was a pleasant and memorable experience. I would also like to show my deepest gratitude to the Yokoyama-Nakajima research group, particularly Professor Yasuhiro Nakajima, for guidance throughout the project.

-
- [1] K. Scholberg, *Annual Review of Nuclear and Particle Science* **62**, 81 (2012).
- [2] A. Mirizzi, I. Tamborra, H.-T. Janka, N. Saviano, K. Scholberg, R. Bollig, L. Hüdepohl, and S. Chakraborty, *La Rivista del Nuovo Cimento* **39**, 1 (2016).
- [3] B. Müller, *Annual Review of Nuclear and Particle Science* **69**, 253 (2019).
- [4] K. Rozwadowska, F. Vissani, and E. Cappellaro, *New Astronomy* **83**, 101498 (2021).
- [5] K. Scholberg, in *Journal of Physics-Conference Series*, Vol. 309 (2011) p. 012028.
- [6] D. Akimov, P. An, C. Awe, P. S. Barbeau, B. Becker, V. Belov, I. Bernardi, M. Blackston, A. Bolozdynya, B. Cabrera-Palmer, *et al.*, *Journal of Instrumentation* **16**, P08048 (2021).
- [7] B. M. Bolotovskii, *Physics-Uspekhi* **52**, 1099 (2009).
- [8] E. Kolbe, K. Langanke, and P. Vogel, *Physical Review D* **66**, 013007 (2002).